

# Ni-W-codoping effects on the optical and structural properties of SnO<sub>2</sub> nanoparticles

A. A. DAKHEL\*

*Department of Physics, College of Science, University of Bahrain, P.O. Box 32038, Zallaq, Kingdom of Bahrain*

Nanoparticles (NPs) of tin oxide codoped with Ni/W ions were synthesized by a co-precipitation technique. The Ni ions molar concentration was fixed at 5% while that of the W ions was varied as, 1.5%, 2.5%, and 3.5%. The present investigation was aimed to study the effect of W doping level on the structural and optical properties of the NPs. The X-ray fluorescence (XRF) technique was performed to check the purity of the nanocrystalline samples. The crystalline structure was investigated by X-ray diffraction (XRD). The results indicate that the Ni/W ions were dissolved in SnO<sub>2</sub> lattice forming a solid solution. The variation of the optical bandgap ( $E_g$ ) of the host SnO<sub>2</sub> NPs was measured by the diffuse reflectance spectroscopy (DRS) as a function of W% doping level. The bandgap was red-shifted that improve the photocatalytic activity under visible light illumination.

(Received July 4, 2022; accepted February 12, 2024)

*Keywords:* Ni/W codoped SnO<sub>2</sub>; TCO; nano particles

## 1. Introduction

Tin oxide (SnO<sub>2</sub>) and other transparent conducting oxides (TCOs: SnO<sub>2</sub>, CdO, TiO<sub>2</sub>, In<sub>2</sub>O<sub>3</sub>, and ZnO) are used in various optoelectronic applications such as solar-cell industries and other field types, such as for gas sensing and photocatalysis [1-3]. SnO<sub>2</sub> usually crystallizes in tetragonal structure (P42/mnm) with lattice parameters  $a=b=0.47382$  nm,  $c=0.31871$  nm. It has semiconducting properties with a wide bandgap of 3.5-3.8 eV [4-8]. Like other TCOs, the physical properties of SnO<sub>2</sub> can be controlled through its structural defects, like tin and oxygen ion interstitials/ vacancies. Therefore, through dilute doping of SnO<sub>2</sub> with dopant ions, the physical properties might be modified and, thus create some controlled interesting exotic properties, like improving its photocatalytic properties or fabricating dilute magnetic semiconductors (DMS) [9-15]. Therefore, Ni/W codoped SnO<sub>2</sub> nanoparticles were synthesized to study the change in the sample structural and optical properties with the variation of W doping level.

The most reliable VI-coordination ionic radii of Sn<sup>4+</sup>, Ni<sup>2+</sup>, and W<sup>6+</sup> are 0.069 nm, 0.069 nm, and 0.06 nm, respectively [16]. Therefore, such close ionic radii indicate that they could easily form substitutional solid solutions (SSS) based on SnO<sub>2</sub>.

## 2. Experimental procedure

Nickel and tungsten ions co-doped SnO<sub>2</sub> nanopowder (abbr. SnO<sub>2</sub>: Ni/ W) samples were synthesized by a thermal co-precipitation technique. The starting materials, tin chloride dihydrate (SnCl<sub>2</sub>.2H<sub>2</sub>O), nickel chloride hexahydrate (NiCl<sub>2</sub>.6H<sub>2</sub>O), and sodium tungstate dihydrate (Na<sub>2</sub>WO<sub>4</sub>.2H<sub>2</sub>O) were used as sources for Sn, Ni, and W

ions, respectively (all used materials were analar-grade from Sigma-Aldrich Chemical Company). The molar ratio of Ni/Sn was fixed at ~5%, meanwhile, the molar ratios of W/Sn in the samples were 1.5%, 2.5%, and 3.5%, respectively. The procedure of synthesis was initiated with ~ 10 ml ethanol mixed with an almost equal amount of deionized water in a glass beaker. Then, controlled amounts of SnCl<sub>2</sub>.2H<sub>2</sub>O, NiCl<sub>2</sub>.6H<sub>2</sub>O, and Na<sub>2</sub>WO<sub>4</sub>.2H<sub>2</sub>O fine powders were added successively to the main solution with a continuous magnetic stirring. Then, ~ 3 drops of concentric HCl acid were added to the solution under magnetic stirring for ~ 2 h, at room temperature. Next, the temperature of the solution was slowly raised to ~ 80°C until formation of a dry powder on the bottom of the beaker. Then, powder was collected, brushed, and flash sintered in the air atmosphere oven at 500°C/ 1h followed by natural cool with the closed oven to room temperature. The formed final formed powder was collected and pelletized for the investigations. A pristine SnO<sub>2</sub> powder was also synthesized by an identical procedure, for comparison. Thus, the synthesised samples were (5%Ni+x%W)-codoped SnO<sub>2</sub>, where the (W/Sn) molar concentration ratio are,  $x=1.5\%$ ,  $2.5\%$ , and  $3.5\%$ , respectively

The elemental content of each synthesized sample was confirmed through the energy-dispersion X-ray fluorescence (XRF) method with an Amptek XR-100CR (USA) detector of XR-detection energy  $\geq 1.7$  keV with an energy resolution 180 eV and controlled by the build-in program, MCDWIN 3.1. The crystalline structures of the samples were investigated by the X-ray diffraction (XRD) method using a Rigaku Ultima-IV diffractometer equipped with Cu  $K_\alpha$  radiation, and the obtained patterns were analyzed by the method of Rietveld profile refinements (RPR) through the built-in PDXL program. The optical

studies were carried out by using a Shimadzu UV-3600 spectrometer supplied with attachments for the diffuse reflectance spectroscopy (DRS) measurements in the 200 – 830 nm range.

### 3. Results and discussion

#### 3.1. Structural analysis

The elemental composition of the synthesized samples (Ni/W-codoped SnO<sub>2</sub>) were confirmed by their XRF spectra, as shown in Fig.1. These XRF spectra show signals from Sn L-band (3.44–3.66 keV), Ni K<sub>α</sub>-signal (7.47 keV), and W L<sub>α</sub>–L<sub>β</sub>-signals (8.39 and 9.67 keV, respectively).

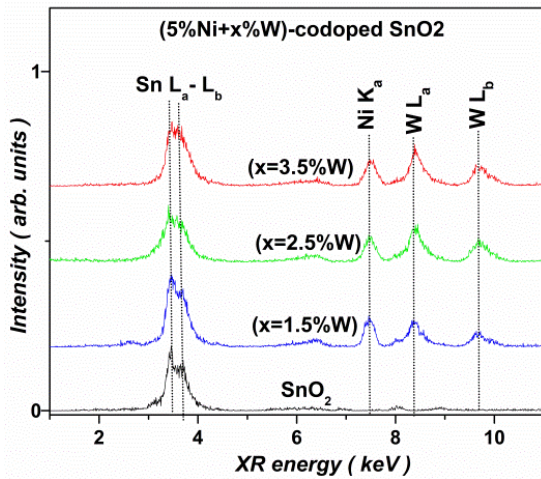


Fig. 1. XRF spectra of the synthesized Ni/W-codoped SnO<sub>2</sub> samples (color online)

The XRD patterns of the synthesized pristine and co-doped Sn oxide samples are shown in Fig.2.

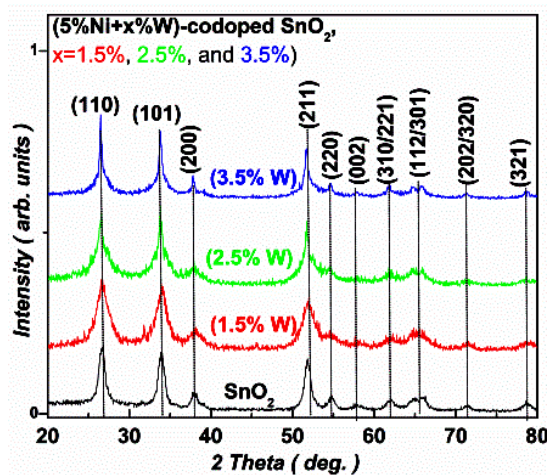


Fig. 2. XRD patterns of the synthesized (5%Ni+x%W)-codoped SnO<sub>2</sub>, where x = 0, 1.5%, 2.5%, and 3.5% nanopowders (color online)

The X-ray diffraction patterns reveal crystallization of a single SnO<sub>2</sub> phase of Cassiterite tetragonal (rutile) structure (P42/mnm) (JCPDS no. 41-1445). The calculated lattice parameters were found to be close to the standard JCPDS data. The crystallite sizes (CS) were estimated by with the Halder-Wagner (H-W) relation [17] to be of nano-size (NCs) as presented in Table 1. The absence of any diffraction peaks from the dopants mostly refers to the incorporation of the dopant ions into the mother lattice of SnO<sub>2</sub>. The calculated fitting RPR parameters ( $R_{wp}$  and  $S$ ) were good enough since  $S$  is close to 1 [18]; It refers also to the almost total incorporation of dopant ions into the crystalline lattice of SnO<sub>2</sub>. The structural data presented in Table 1, show that the present doping of SnO<sub>2</sub> crystal slightly reduced the unit-cell volume ( $V_{cell}$ ), which is attributed to the correct substitutional doping. The CS results given in Table 1 show that the present doping reduced the crystallinity; however, the crystallinity was slightly improved with increasing of the W% doping level. In general, the inclusion of Ni/W ions should create some structural strain,  $\epsilon_s$ :  $\epsilon_s = -\Delta\theta_{(110)} \cot \theta_{(110)}$ , where  $\Delta(2\theta_{110})$  is the angular shift of the (110)-intensive reflection due to the Ni/W inclusion, relative to that of pristine SnO<sub>2</sub>. The results are presented in Table 1, which disclosed that the structural strain  $\epsilon_s$  was increased by increasing of W% doping level as a result of the ionic radii difference. According to H-R rules, the Ni and W doped ions can diffuse into the SnO<sub>2</sub> lattice structure medium forming SSS. Accordingly, the average nanometric crystallite size (CS) of SnO<sub>2</sub> was reduced by ~40% (Table 1).

#### 3.2. Optical analysis

The spectral diffuse reflectance,  $R(\lambda)$  of the synthesized NPs was measured in the range of 200–800 nm to investigate the optical properties including the bandgap,  $E_g$ . The spectral absorption function,  $F(\lambda)$  of each sample was calculated through the Kubelka-Munk (K-M) relation;  $F=[1-R]^2/2R$  [19], and the results are shown graphically in Fig. 3.

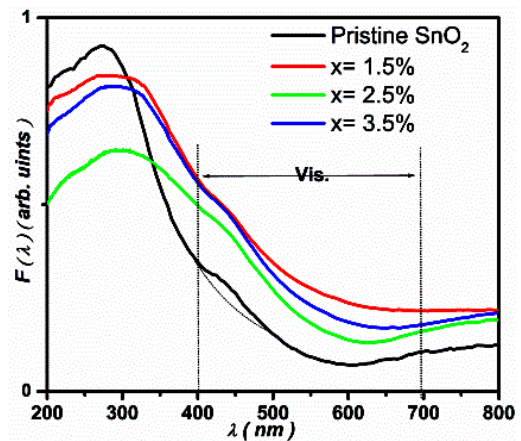


Fig. 3. Wavelength dependence of the Spectral absorption function  $F(\lambda)$  of the synthesized Ni/W-codoped SnO<sub>2</sub> samples (color online)

Thus, the absorption spectra of the host SnO<sub>2</sub> samples did not qualitatively change under the current dilute doping. Generally, the spectral function  $F(\lambda)$  of the present samples has a main absorption band for  $\lambda < 400$  nm. The enhancement of the absorption in the visible region (fig. 3) is attributed to the increase in the concentration of the Sn- and O- ion vacancies in the crystal as a consequence of doping that leads to a redshift in the bandgap [20].

The absorption function  $F(\lambda)$  is used to determine the direct optical bandgap ( $\varepsilon_g$ ) by using Tauc

equation;  $[F(\lambda) \times \varepsilon]^2 = C_{op} (\varepsilon - \varepsilon_g)$  [21], where  $C_{op}$  is the sample's optical constant and  $\varepsilon = h\nu$  is the photon energy. Thus, the plot  $[F(\lambda) \times \varepsilon]^2$  vs.  $\varepsilon$  is used to find the gap  $\varepsilon_g$  following Tauc technique, as shown in Fig.4, and the results are presented in Table 1.

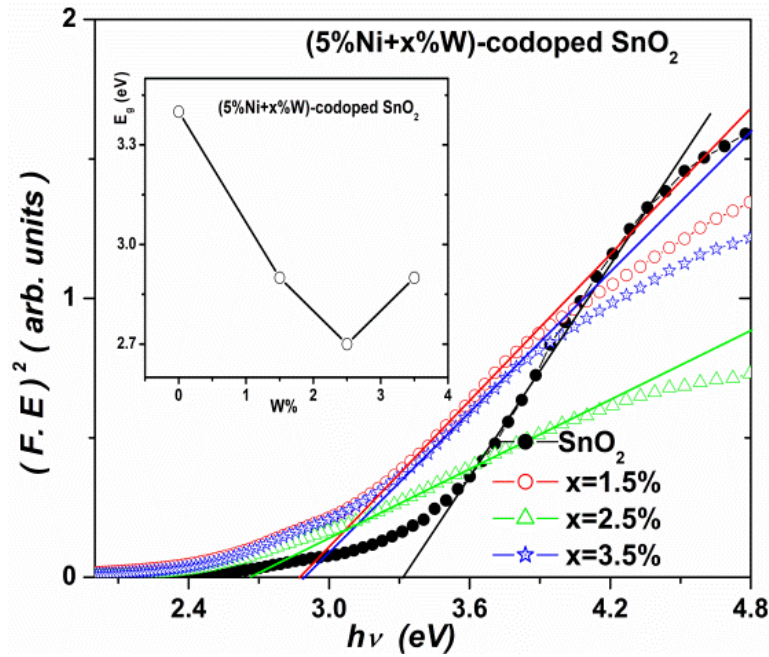


Fig. 4. Tauc plots for the synthesized Ni/W-codoped SnO<sub>2</sub> samples. The inset shows the W%-doping level dependent of the bandgap of the synthesized samples (color online)

The obtained bandgap (3.4 eV) for the pristine nano SnO<sub>2</sub> agrees well with the previously measured values (3.5–3.8 eV). The broad range of bandgap values was reported depending on the sample synthesis conditions, as discussed in ref. [22]. However, the bandgap of pristine SnO<sub>2</sub> is quite higher than that of the doped samples, revealing large changes in the band structure caused by dilute doping. As the bandgap (table 1) of the host SnO<sub>2</sub> became in the visible range, the present doping can be used to improve the photocatalytic activity of SnO<sub>2</sub> under visible light.

The bandgap of a TCO is usually influenced by consequences of the doping process that narrows the bandgap (Urbach effect [23]), which is observed in the present work (Table 1). The narrowing of the bandgap of host SnO<sub>2</sub> by doping can be explained by the generation of structural point defects including O-vacancies of energy levels that lay in the bandgap and merged with the host SnO<sub>2</sub> conduction band, causing a decrease in the bandgap, according to the Urbach effect. Such large change in the bandgap of host SnO<sub>2</sub> due to different dopings was also measured in different works [24–27].

Table 1. Lattice structural strain ( $\varepsilon$ ), Crystallite size (CS), Lattice parameters ( $a=b$  and  $c$ ), unit-cell volume ( $V_{cell}$ ), Rietveld refinement parameters ( $R_{wp}(\%)$ : the weighted profile factor and  $S(\%)$ : the goodness-of-fit parameter) and the optical bandgap ( $E_g$ ) of the synthesized nanoparticle samples

Sample	$\varepsilon$	CS(nm)	Lattice parameters $a=b$ (Å) $c$ (Å)		$V_{cell}(\text{Å}^3)$	$R_{wp}$ (%)	$S$ (%)	$E_g$ (eV)
SnO <sub>2</sub>	Ref.	8.8	4.7421	3.190	71.73	13.03	1.11	3.4
SnO <sub>2</sub> :Ni:1.5%W	0.08	5.0	4.741	3.192	71.75	17.6	1.05	2.9
SnO <sub>2</sub> :Ni:2.5%W	0.13	5.1	4.742	3.1855	71.62	16.99	1.09	2.7
SnO <sub>2</sub> :Ni:3.5%W	0.23	6.2	4.742	3.184	71.58	18.31	1.19	2.9

#### 4. Conclusions

Pristine and Ni/W codoped SnO<sub>2</sub> NPs were successfully synthesized by the co-precipitation method. The codoping of Ni/W ions into SnO<sub>2</sub> lattice was confirmed by the detailed studies of the structural/optical properties and explained by Hume-Rothery rules. With the increasing W% doping level, the nano CS and structural strain ( $\epsilon$ ) increased, which was attributed to the ionic radii differences. The increase of the unit-cell volume with increasing of W% doping level was mainly attributed to the creation of O-vacancies. The creation of O-vacancies causes the present redshift of the bandgap. Moreover, as the bandgap of the host SnO<sub>2</sub> become in the visible range, the present doping can be adopted to improve the photocatalytic activity under visible light illumination.

#### References

- [1] B. Roose, C. M. Johansen, K. Dupraz, T. Jaouen, P. Aebi, U. Steiner, A. Abate, *J. Mater. Chem. A* **6**(4), 1850 (2018).
- [2] G. Singh, R. C. Singh, *J. Electron. Mater.* **48**(7), 478 (2019).
- [3] Luis Castañeda, *Mater. Sci. Applications* **2**, 1233 (2011).
- [4] C. B. Fitzgerald, M. Venkatesan, L. S. Dorneles, R. Gunning, P. Stamenov, J. M. D. Coey, P. A. Stampe, R. J. Kennedy, E. C. Moreira, U. S. Sias, *Phys. Rev. B* **74**, 115307 (2006).
- [5] J. Hays, A. Punnoose, R. Baldner, M. H. Engelhard, J. Peloquin, K. M. Reddy, *Phys. Rev. B* **72**, 075203 (2005).
- [6] S. B. Ogale, R. J. Choudhary, J. P. Buban, S. E. Lofland, S. R. Shinde, S. N. Kale, V. N. Kulkarni, J. Higgins, C. Lanci, J. R. Simpson, N. D. Browning, S. Das Sarma, H. D. Drew, R. L. Greene, T. Venkatesan, *Phys. Rev. Lett.* **91**, 077205 (2003).
- [7] M. A. Maki-Jaskari, T. T. Rantala, *Phys. Rev. B* **64**, 075407 (2001).
- [8] H. A. Mohamed, N. M. A. Hadia, *Int. J. Thin Fil. Sci. Tec.* **4**(1), 1 (2015).
- [9] A. Bouaine, N. Brihi, G. Schmerber, C. Ulhaq-Bouillet, S. Colis, A. Dinia, *J. Phys. Chem. C* **111**, 2924 (2007).
- [10] A. A. Dakhel, A. R. AlBasri, M. A. Khunji, *J. Supercond. Nova. Magn.* **32**, 651 (2019).
- [11] A. A. Dakhel, M. El-Hilo, M. Bououdina, *Adv. Power Tech.* **25**, 1839 (2014).
- [12] A. A. Dakhel, H. Hamad, Adnan Jaafar, *J. Supercond. Nova. Magn.* **32**, 253 (2019).
- [13] M. El-Hilo, A. A. Dakhel, Z. J. Yacoob, *J. Magn. Mater.* **482**, 125 (2019).
- [14] A. A. Dakhel, *Appl. Phys. A* **123**(214), 2 (2017).
- [15] K. Singh, I. Rawal, P. Gautam, N. Sharma, R. Dhar, *J. Magn. Mater.* **468**, 259 (2018).
- [16] R. D. Shannon, *Acta Crystallogr. A* **32**, 751 (1976).
- [17] Fujio Izumi, Tajuji Ikeda, Annual report Advanced Ceramics Research Centre Nagoya Institute of Technology **3**, 33 (2015).
- [18] L. B. McCusker, R. B. Von Dreele, D. E. Cox, D. Louer, P. Scardi, *J. Appl. Cryst.* **32**, 36 (1999).
- [19] A. E. Morales, E. S. Mora, U. Pal, *Revista Mexicana de Fisica* **S53**, 18 (2007).
- [20] Wei Zhou, Lijuan Liu, Mengying Yuan, Qinggong Song, Ping Wua, *Computational Materials Science* **54**, 109 (2012).
- [21] J. Tauc, F. Abelesn (ed.), *Optical Properties of Solids*, North Holland, 1969.
- [22] S. Dalui, S. Rout, A.J. Silvestre, G. Lavareda, L. C. J. Pereira, P. Brogueira, O. Conde, *Appl. Surf. Sci.* **278**, 127 (2013).
- [23] F. N. C. Anyaegbunam, C. Augustine, *Dig. J. Nanomater. Bios.* **13**, 847 (2018).
- [24] J. Divya, A. Pramothkumar, S. Joshua Gnanamuthu, D. C. Bernice Victoria, P. C. Jobe Prabakar, *Physica B* **588**, 412169 (2020).
- [25] A. A. Dakhel, *Mater. Chem. and Phys.* **252**, 123163 (2020).
- [26] A. S. Ahmed, A. Azam, M. Shafeeque, M. Chaman, S. Tabassum, *J. Phy. Chem. Sol.* **73**, 943 (2012).
- [27] R. Kumar, F. Singh, B. Angadi, W. K. Choi, K. Jeong, J- H. Song, M. W. Khan, J. P. Srivastava, A. Kumar, R. P. Tandon, *J. Appl. Phys.* **100**, 113708 (2006).

\*Corresponding author: adakhil@uob.edu.bh